applied sciences

MDPI

Article

Measurements of the Magnetic Field Variations Related with the Size of V-Shaped Notches in Steel Pipes

J. Jesús Villegas-Saucillo [1], José Javier Díaz-Carmona [1], Marco A. Escarola-Rosas [2], Héctor Vázquez-Leal [3,4], Jaime Martínez-Castillo [5] and Agustín L. Herrera-May [2,5,*]

1 Instituto Tecnológico de Celaya, Celaya 38020, Mexico; jesus.villegas@itcelaya.edu.mx (J.J.V.-S.); javier.diaz@itcelaya.edu.mx (J.J.D.-C.)
2 Maestría en Ingeniería Aplicada, Facultad de Ingeniería de la Construcción y el Hábitat, Universidad Veracruzana, Boca del Río 94294, Mexico; maerescarola@gmail.com
3 Electronic Instrumentation and Atmospheric Sciences School, Universidad Veracruzana, Xalapa 91000, Mexico; hvazquez@uv.mx
4 Consejo Veracruzano de Investigación Científica y Desarrollo Tecnológico (COVEICYDET), Xalapa 91069, Mexico
5 Micro and Nanotechnology Research Center, Universidad Veracruzana, Boca del Río 94294, Mexico; jaimartinez@uv.mx
* Correspondence: leherrera@uv.mx; Tel.: +52-229-7752-000

Abstract: Gas and oil pipeline networks require periodic inspections to detect cracks or notches that can cause industrial accidents and environmental contamination. For these inspections, the metal magnetic memory (MMM) method could be used as a non-destructive testing (NDT) technique, which does not need expensive equipment and high-skilled operators. However, more investigations are required to quantify the size and shape of defects in ferromagnetic pipes using the MMM signals. We present experimental measurements of MMM signals around five small V-shaped notches of an ASTM-A36 steel pipe using a three-axis magnetoresistive sensor. The V-shaped notches have different values of depth (500 μm, 1000 μm, 1500 μm, 2000 μm and 2500 μm) and width (1000 μm, 1500 μm, 2000 μm, 3000 μm and 3500 μm). We measured the variations of tangential and normal MMM signals around these defects and their relationships with the size of each defect. The first V-notch defect (500 μm depth and 1000 μm width) registers variations of the tangential and normal MMM signals of 14.32 μT ± 1.62 μT and 27.95 μT ± 1.14 μT, respectively. On the other hand, the fifth V-notch defect (2500 μm depth and 3500 μm width) has variations of the tangential and normal MMM signals of 68.75 μT ± 1.10 μT and 71.37 μT ± 0.72 μT, respectively. The MMM method could be used for real-time monitoring of V-shaped notches in steel pipes. This method does not require special treatment of steel pipes.

Keywords: gas and oil pipeline network; magnetic field variations; metal magnetic memory method; magnetometer; non-destructive testing; V-shaped notches

Citation: Villegas-Saucillo, J.J.; Díaz-Carmona, J.J.; Escarola-Rosas, M.A.; Vázquez-Leal, H.; Martínez-Castillo, J.; Herrera-May, A.L. Measurements of the Magnetic Field Variations Related with the Size of V-Shaped Notches in Steel Pipes. *Appl. Sci.* **2021**, *11*, 3940. https://doi.org/10.3390/app11093940

Academic Editor: Giuseppe Lacidogna

Received: 5 February 2021
Accepted: 21 April 2021
Published: 27 April 2021

1. Introduction

Gas and oil pipeline networks need periodic inspections for monitoring defects that can generate damages to the surrounding environment [1,2]. Early detection of these defects could help avoid accidents in a pipeline [3,4]. These defects can be measured using non-destructive testing (NDT) techniques, such as ultrasonic testing, Eddy current testing, X-ray inspection, liquid penetrant test, thermography, and magnetic flux leakage testing [5–9]. For instance, ultrasonic testing can detect small flaws in pipes using ultrasonic pulses. However, this NDT technique requires operators with high technical experience [10,11]. Another NDT technique is Eddy current testing, which is used for monitoring defects in ferromagnetic pipes based on electromagnetic induction [12–14]. This technique requires external magnetic field sources and high-skilled operators in order

to acquire the measurements. In addition, X-ray inspections can detect small flaws of pipes using expensive equipment and operators with extensive technique experience [15,16]. On the other hand, liquid penetrant testing can be employed for inspections of pipes using liquids around defects. However, this NDT technique requires pipes with surfaces free of contaminants [17]. Additionally, magnetic flux leakage testing uses an external source of magnetic flux close to surface of ferromagnetic pipes, in which the magnetic field changes around discontinuities [18,19]. Several of these NDT techniques need special treatment on the surfaces of pipes and expensive equipment. In addition, several of these techniques have problems for real-time monitoring of defects in ferromagnetic pipes.

An alternative NDT technique is the metal magnetic memory (MMM) method, which could be used for real-time monitoring of defects in ferromagnetic samples [20,21]. This method is based on the self-magnetization field of ferromagnetic samples [22,23]. The MMM method can be used for detecting early damage to ferromagnetic structures [24,25]. It is mainly used in soft ferromagnetic materials, such as medium carbon steel [26]. This method does not require an external magnetic field source, expensive equipment and special treatment on the surfaces of samples. The MMM method can be used to detect cracks in ferromagnetic structures, based on variations in residual magnetic field signals. Generally, the MMM method is employed to detect the locale of surface defects in ferromagnetic materials. However, the MMM method requires more investigations regarding the quantitative relations between the shape and size of the defects, and the variations of their tangential and normal MMM signals. A few investigations [27] have been reported about MMM signals around V-shaped notches in steel pipes. In order to study the behavior of the MMM signals of V-shaped notches, we measured the tangential and normal MMM signals around five different V-shaped notches in an ASTM-A36 steel pipe. These signals were obtained using a rotatory system, a commercial three-axis magnetoresistive sensor MAG3110 (Austin, Texas, USA, Freescale semiconductor), a mega Arduino board and a laptop. The tangential and normal MMM signals registered variations due to changes in the size (depth and width) of the V-shaped notches. This MMM method could be used for real-time monitoring of small V-shaped notches (with a minimum size of a few hundred micrometers) in oil and gas pipelines using low-cost equipment and without high-skilled operators.

This paper is structured as follows: Section 2 describes the main parameters of the five different V-shaped notches on surface of an ASTM-A36 steel pipe and the experimental setup. Section 3 presents the results and discussions of the MMM signals related with the V-shaped notches. Section 4 describes the conclusions and future work.

2. Materials and Methods

In this section, we depict the experimental setup and main parameters of five V-shaped notches in an ASTM-A36 steel pipe.

Figure 1 shows an ASTM-A36 steel pipe (280 mm length, 89 mm outer diameter and 5.45 mm thickness) that has five different V-shaped notches on its outer surface. The dimensions of the five V-shaped notches are shown in Table 1. The first notch has minimum values of 1000 μm width and 500 μm depth. The fifth notch however has maximum dimensions of 3500 μm width and 2500 μm depth.

Table 1. Dimensions of five V-shaped notches on the surface of an ASTM-A36 steel pipe.

V-Notch Defect	Width (μm)	Depth (μm)
S1	1000.0	500.0
S2	1500.0	1000.0
S3	2000.0	1500.0
S4	3000.0	2000.0
S5	3500.0	2500.0

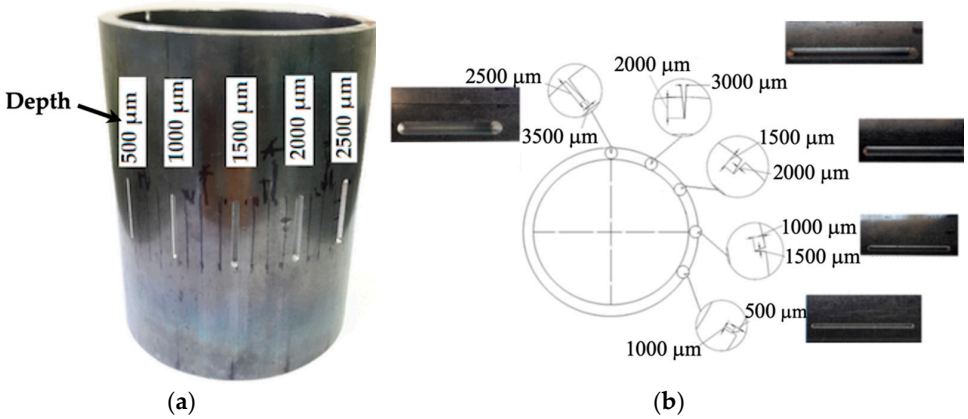

Figure 1. Five V-shaped notches (**a**) of different widths and depths (1000 µm × 500 µm, 1500 µm × 1000 µm, 2000 µm × 1500 µm, 3000 µm × 2000 µm, and 3500 µm × 2500 µm) on the outer surface and (**b**) along the perimeter of an ASTM-A36 steel pipe.

Figure 2 depicts the experimental setup to measure the MMM signals around five small V-shaped notches on the outer surface of an ASTM-A36 steel pipe. This system contains a rotational mechanism; a (2 mm × 2 mm × 0.85 mm) commercial three-axis magnetoresistive sensor MAG3110 (Austin, Texas, USA, Freescale semiconductor) of high sensitivity (0.1 µT), an Arduino mega 2560 (Santiago, Chile, Arduino) and data processing through an Arduino board. The rotational mechanism uses a motor with encoder (12 VDC precision Faulhaber model 2342L012CR, Clearwater, Florida, USA) that generates a rotational motion of 2 rpm. In addition, the mechanical structure of the rotational mechanism is fabricated with non-magnetic materials, such as nylamide and aluminum. Thus, the residual magnetic field of the pipe is not affected by the rotational mechanism. The steel pipe is collocated in the rotational mechanism, which is supplied with a DC power supply (B&K Precision 1761, Yorba linda, California, USA). The magnetoresistive sensor employs an I^2C (inter-integrated circuit protocol) interface to communicate with Arduino mega. The distance between the magnetoresistive sensor and the outer surface of each steel pipe was kept constant at 2 mm. This distance must have a minimum value to ensure a better detection of the magnetic signals around the defects. This is due to the fact that the magnitudes of these signals significantly decrease with an increase in the distance with respect to the surface of the steel pipe. Thus, the MMM method is most sensitive for monitoring small variations of the magnetic fields close to defects on the steel pipe. The measured MMM signals around the five V-shaped notches in the steel pipe are processed using a laptop with MATLAB software. The proposed system has a simple operation that can measure tangential and normal MMM signals of the V-shaped notches on the surface of an ASTM-A36 steel pipe.

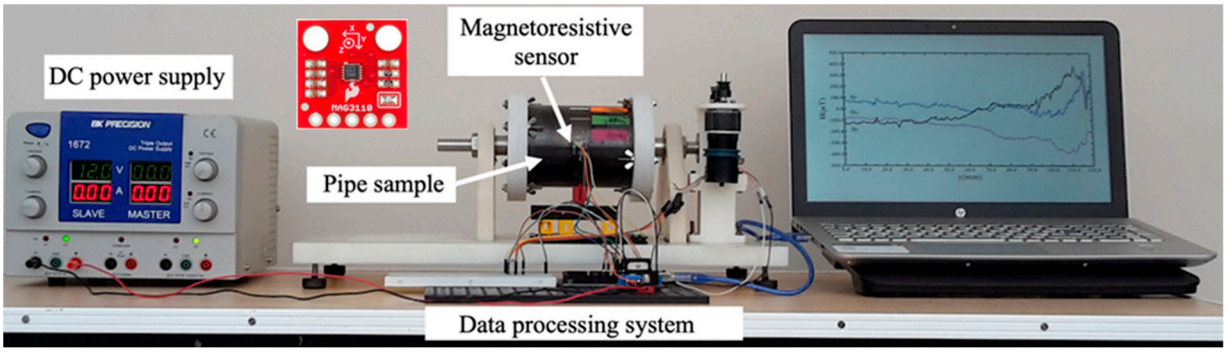

Figure 2. Measurement system of tangential and normal MMM signals around five different V-notch defects on the outer surface of an ASTM-A36 steel pipe.

3. Results and Discussion

This section includes the experimental results of tangential and normal MMM signals around five V-shaped notches in an ASTM-A36 steel pipe. The relations between these MMM signals and the size of the notches are studied. The MMM signals are measured along the perimeter of the steel pipe. We measured the tangential and normal MMM signals around each defect, considering a separation distance (z) between −2 mm and 2 mm. Figure 3 shows six measurements of tangential MMM signals around first V-shaped notch (S1). These MMM signals registered a minimum peak (−252.83 μT ± 1.39 μT) close to the defect center (z = 0 mm). This MMM signal describes a behavior similar to a U-shaped curve. The tangential MMM signal reached its maximum variation (14.32 μT ± 1.62 μT) at the defect center. This maximum variation is related to the depth (500 μm) of the defect on the outer surface of the pipe. In addition, Figure 4 illustrates the normal MMM signals close to the first notch (S1). Due to the two edges around the notch center, the normal MMM signals present two peak values, a maximum peak (71.22 μT ± 0.66 μT) before the notch center and a minimum peak (43.27 μT ± 0.52 μT) after the notch center. This normal MMM response shows a change in its variation direction close to the notch center. This change in variation direction is related to the curvature shift of the normal MMM signal, similar to that represented by an inflection point. These two peaks have a separation distance, parallel to the z-axis, that is related to a notch width of 1000 μm. Thus, the depth and width of the V-shaped notch alter the behavior of the tangential and normal MMM signals, respectively. However, the measured curves are not symmetric around the z = 0 of each defect. This could be caused by the influence of the self-magnetic field along the perimeter of the pipe related with the stress state of the material.

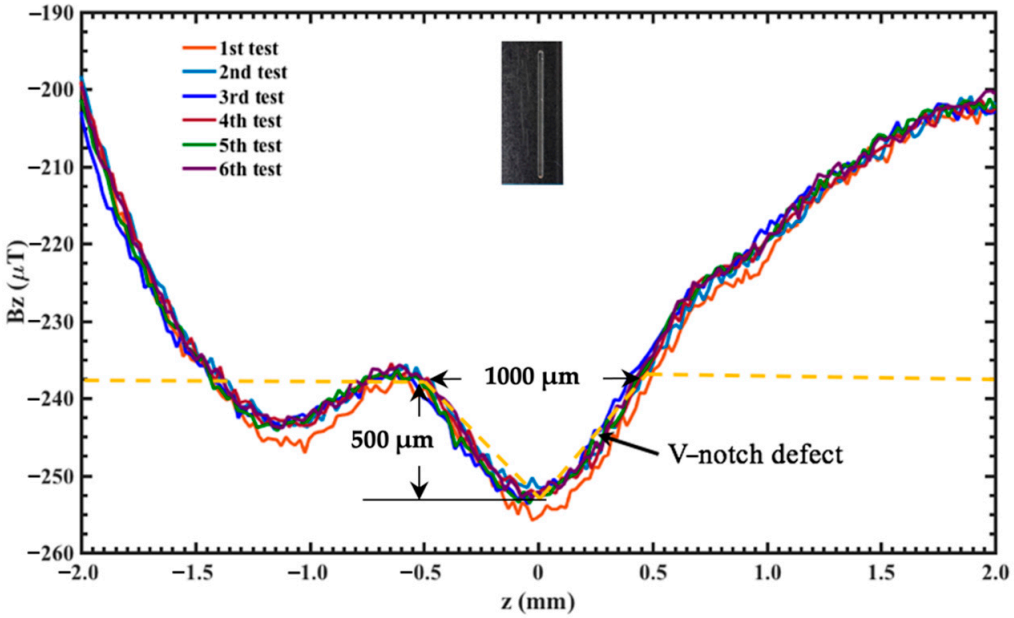

Figure 3. Variation of tangential MMM signals around the first V-shaped notch (1000 μm width and 500 μm depth) of the ASTM-A36 steel pipe, which were measured using six experimental tests.

Figure 5 shows six measurements of tangential MMM signals around the second V-shaped notch (S2), which registered a minimum peak (–224.38 μT ± 1.31 μT) close to the defect center (z = 0 mm). Before this defect, the value of the tangential MMM signal decreased achieving its minimum magnitude near the notch center. After the defect center, the tangential MMM response increased. The magnetic field shift was caused by the defect depth (1000 μm) along the outer surface of the pipe, registering a maximum variation (16.08 μT ± 1.86 μT) at the notch center. Six measurements of normal MMM signals around the second notch (S2) are shown in Figure 6. Before the first edge of the second notch,

the normal MMM signals had values close to 113.80 ± 0.28 μT. After the first edge of this defect, these signals decreased to 87.40 μT ± 0.40 μT at the second edge of the notch. The width (1500 μm) of the second notch affected the magnetic signal shift along a distance close to 1.5 mm.

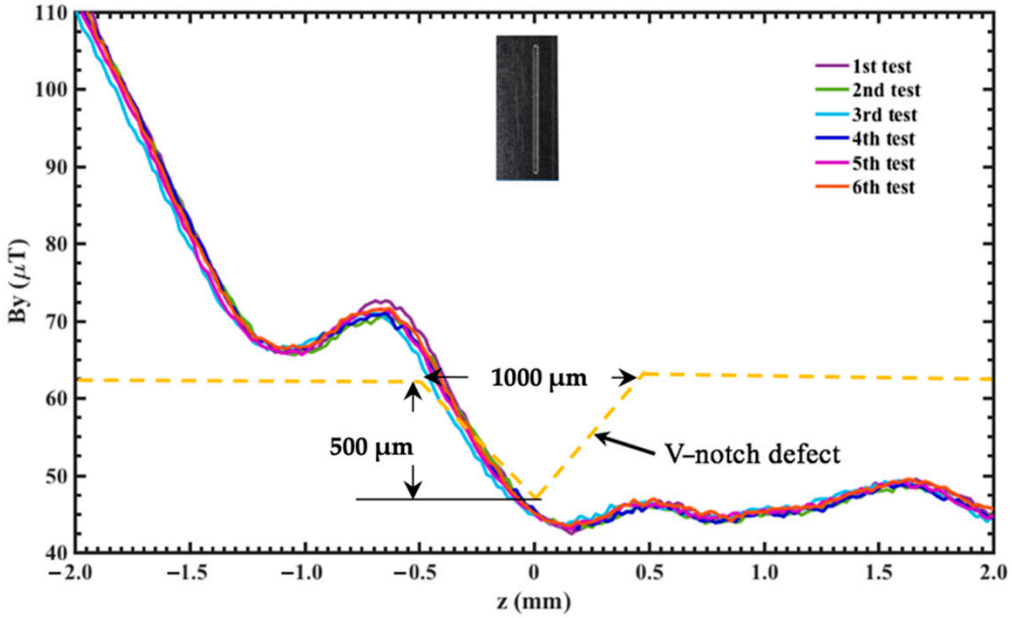

Figure 4. Variation of normal MMM signals around the first V-shaped notch (1000 μm width and 500 μm depth) of the ASTM-A36 steel pipe, which were measured using six experimental tests.

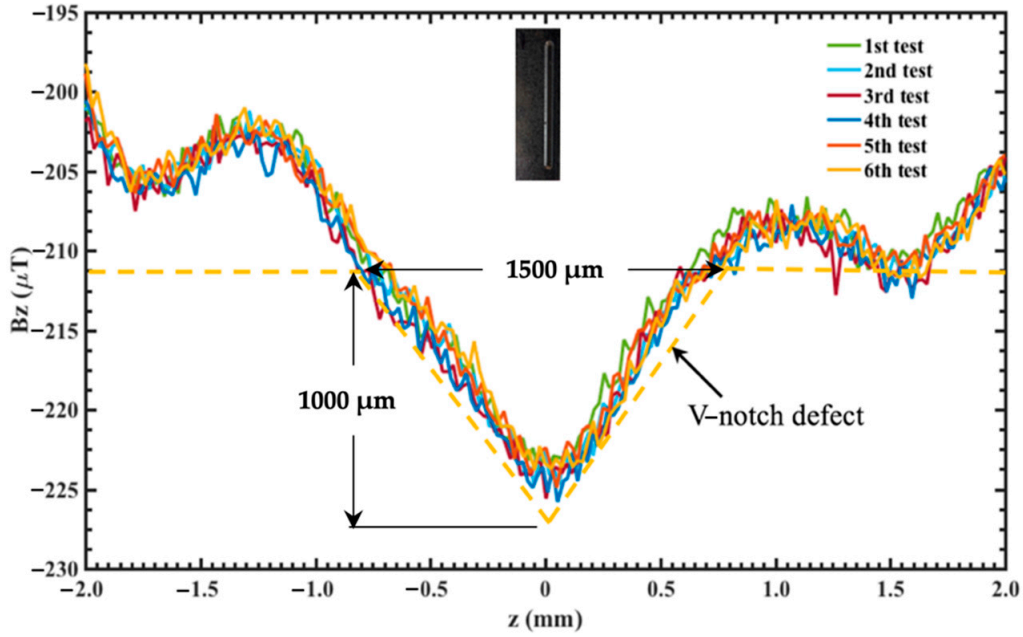

Figure 5. Variation of tangential MMM signals measured around the second V-shaped notch (1500 μm width and 1000 μm depth) of the ASTM-A36 steel pipe, which were measured using six experimental tests.

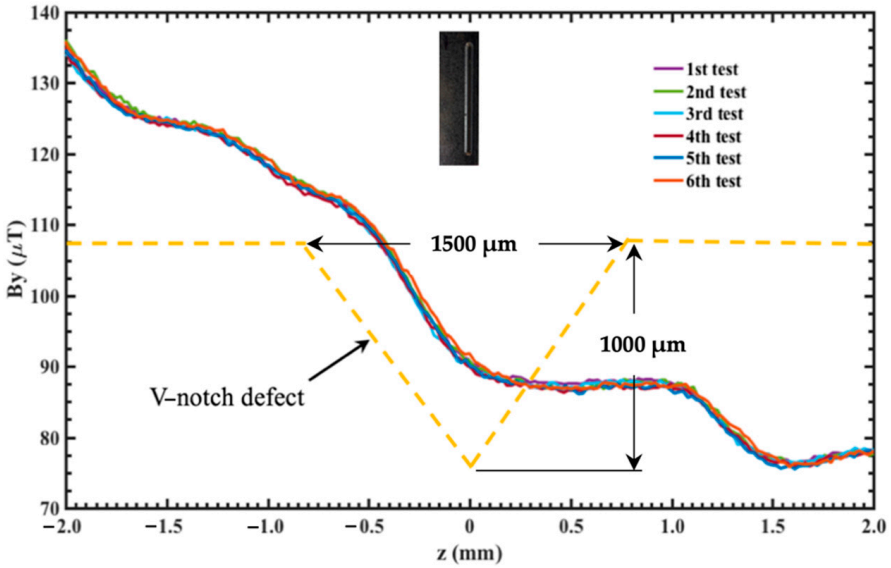

Figure 6. Variation of normal MMM signals measured around the second V-shaped notch (1500 µm width and 1000 µm depth) of the ASTM-A36 steel pipe, which were measured using six experimental tests.

For the third V-shaped notch (S3), six measurements of tangential MMM signals registered a minimum peak (−202.90 µT ± 0.90 µT) near the notch center (z = 0 mm). This peak was due to the depth (1500 µm) of the third notch, as shown in Figure 7. Along the surface perimeter of the pipe, the tangential MMM response decreased at the defect center. The maximum variation of the tangential MMM signal around defect center was 66.73 µT ± 1.13 µT. Figure 8 depicts six measurements of normal MMM signals of this third notch, in which these signals have a shift in their variation direction close to the defect center. Near the first edge of this notch, the normal MMM responses achieved a maximum peak of 159.32 µT ± 0.48 µT. On the other hand, around the second edge, the normal MMM signals had a minimum value of –96.68 µT ± 0.26 µT. The difference between these two values occurs along an approximate distance of 2 mm, which is related to the width (2000 µm) of the third notch (S3).

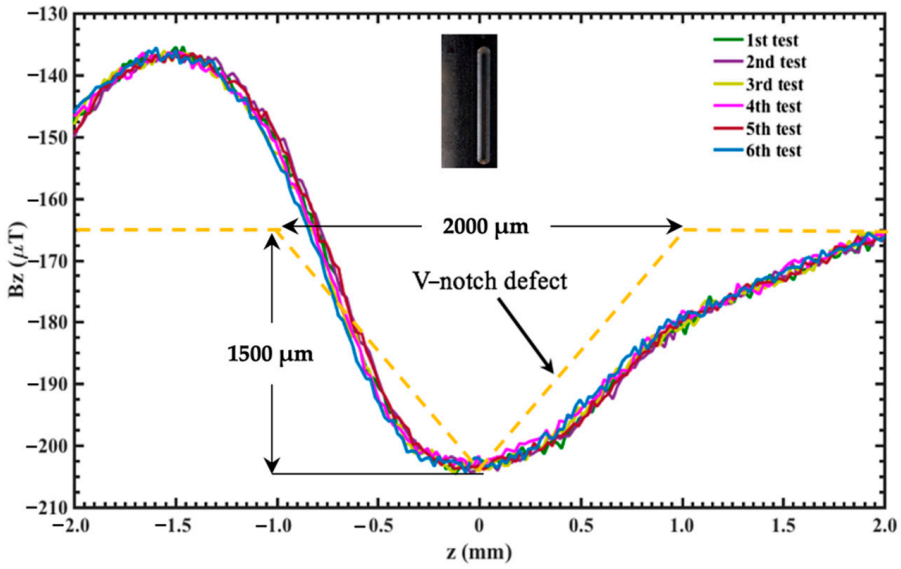

Figure 7. Variation of tangential MMM signals measured around the third V-shaped notch (2000 µm width and 1500 µm depth) of the ASTM-A36 steel pipe, which were measured using six experimental tests.

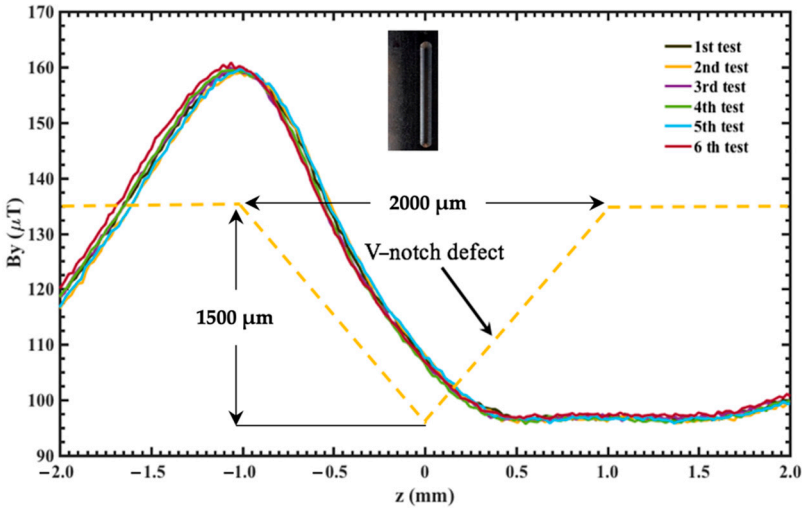

Figure 8. Variation of normal MMM signals measured around the third V-shaped notch (2000 μm width and 1500 μm depth) of the ASTM-A36 steel pipe, which were measured using six experimental tests.

Figures 9 and 10 illustrate six measurements of tangential and normal MMM signals of the fourth V-shaped notch (S4). The tangential MMM signals registered a minimum peak value of −162.40 μT ± 1.33 μT close to the notch center (z = 0 mm). Thus, the maximum shift of the tangential MMM signal is 55.13 μT ± 1.33 μT around defect center. This variation is due to the notch depth (2000 μm) of the pipe surface. Furthermore, the normal MMM response has a change in its variation direction near to defect center, which is related with the two edges of the fourth defect (3000 μm width). In addition, Figures 11 and 12 show six measurements of tangential and normal MMM signals about fifth V-shaped notch (S5). A minimum peak value (−157.27 μT ± 0.94 μT) of the tangential MMM response is measured along the notch center (z = 0 mm) and is related with to notch depth (2500 μm depth). The maximum change of the tangential MMM signal around the defect center is 68.75 μT ± 1.10 μT. On the other hand, the normal MMM signals has maximum and minimum values of 155.17 μT ± 0.43 and 83.80 μT ± 0.41 μT, respectively. These normal MMM signals registered a change in their variation direction close to the notch center. Thus, the measurement of the tangential and normal MMM signals can be used to quantify the size (depth and width) of the V-shaped notch.

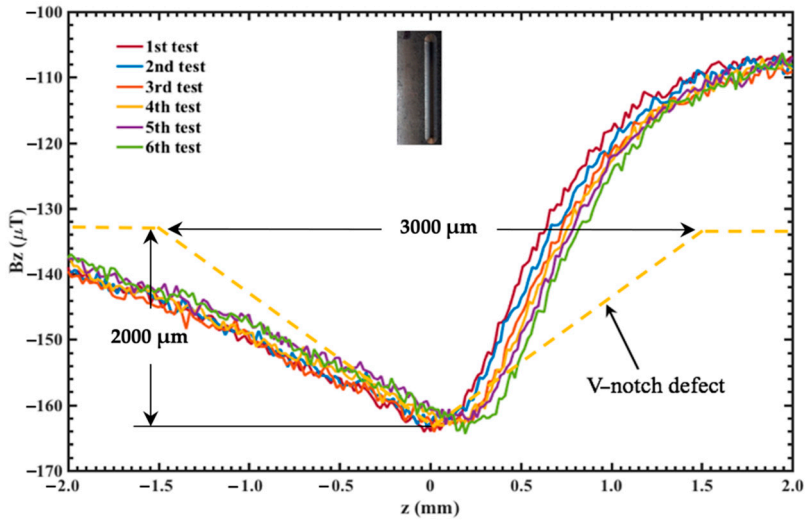

Figure 9. Variation of tangential MMM signals measured around the fourth V-shaped notch (3000 μm width and 2000 μm depth) of the ASTM-A36 steel pipe, which were measured using six experimental tests.

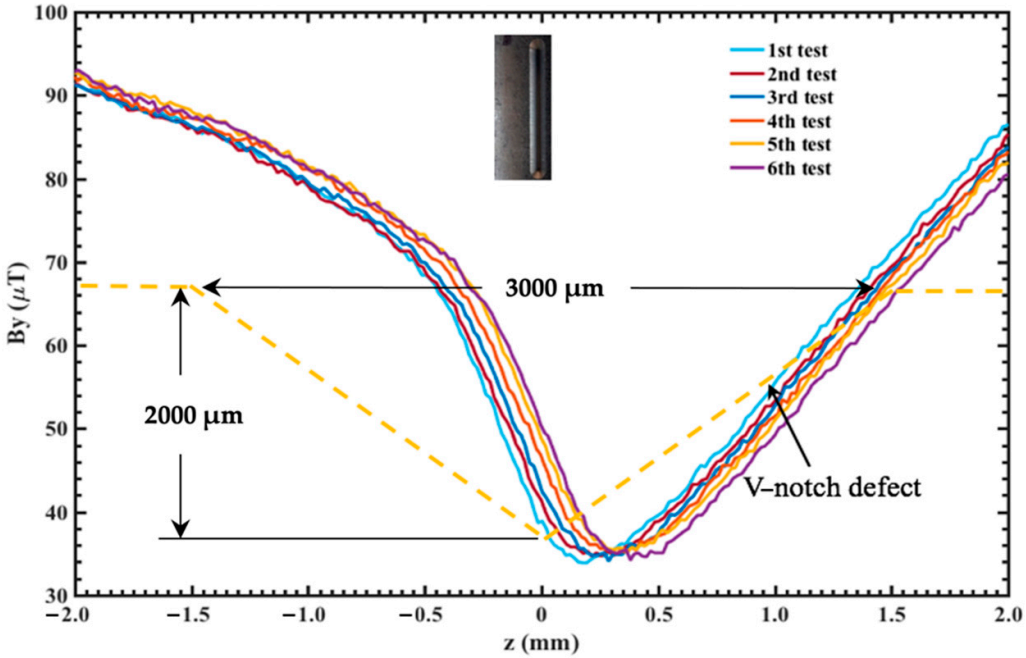

Figure 10. Variation of normal MMM signals measured around the fourth V-shaped notch (3000 µm width and 2000 µm depth) of the ASTM-A36 steel pipe, which were measured using six experimental tests.

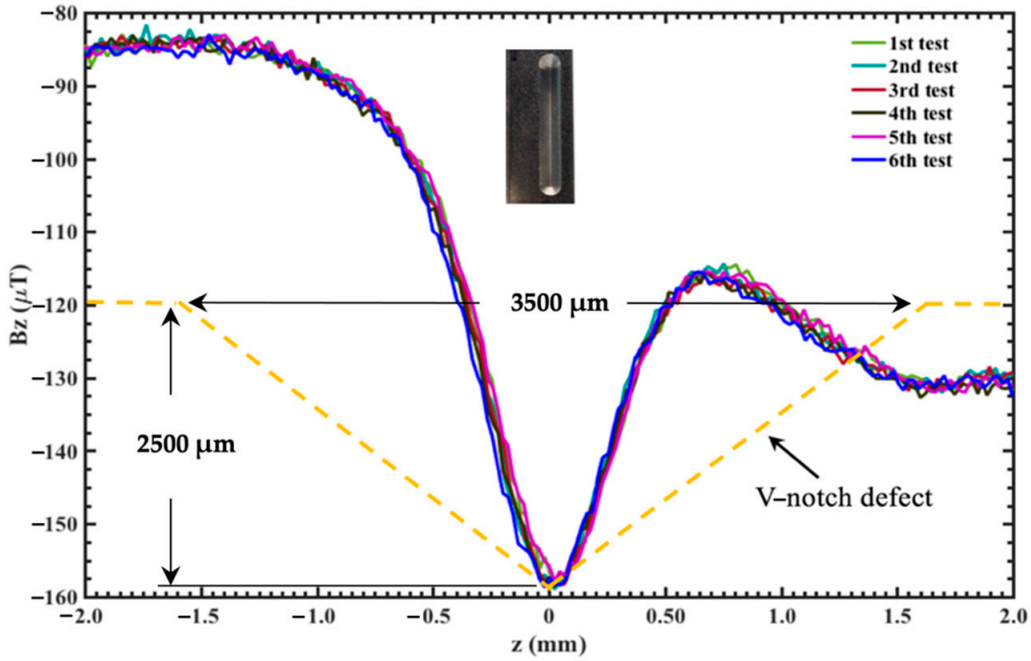

Figure 11. Variation of tangential MMM signals measured around the fifth V-shaped notch (3500 µm width and 2500 µm depth) of the ASTM-A36 steel pipe, which were measured using six experimental tests.

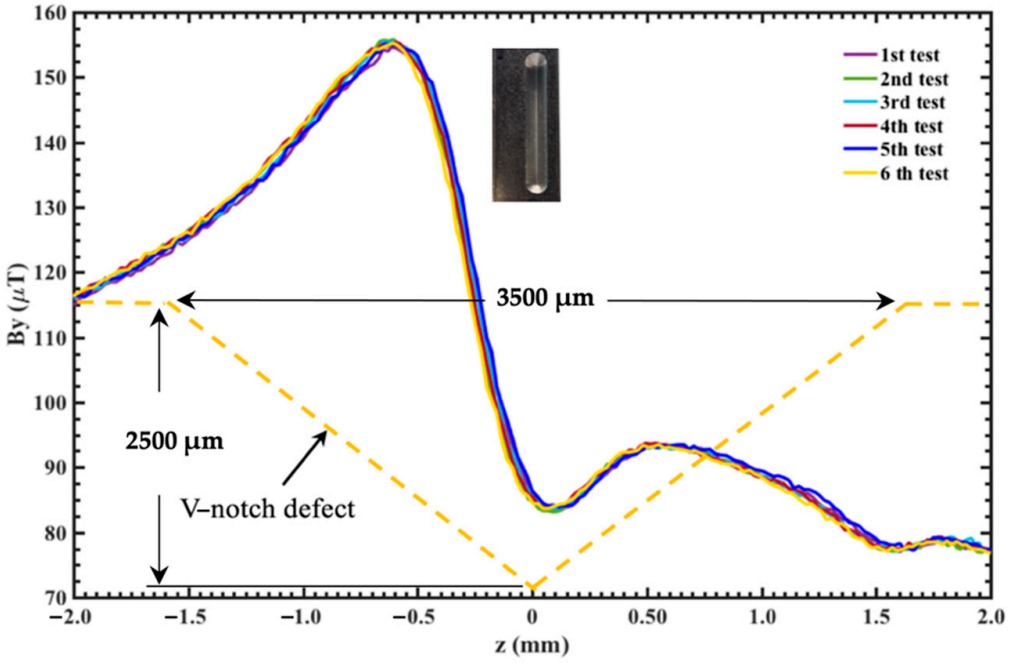

Figure 12. Variation of normal MMM signals measured around the fifth V-shaped notch (3500 µm width and 2500 µm depth) of the ASTM-A36 steel pipe, which were measured using six experimental tests.

Table 2 indicates the values of minimum tangential MMM signals at the center of the V-shaped notches, as well as the maximum and minimum normal MMM signals at the edges of each notch. Furthermore, the maximum variations of tangential MMM signals around five notches are indicated in Table 3. Tangential MMM signals had variations of 14.32 µT ± 1.62 µT and 16.08 µT ± 1.86 µT close to center of the first and second notches, respectively. Moreover, the third notch shows a higher tangential MMM signal shift (66.73 µT ± 1.13 µT) in comparison with those of the first two defects. In the fourth notch, we observed a tangential MMM signal variation of 55.13 µT ± 1.33 µT, which is higher than those of the first and second notch. The fifth notch had a change of tangential MMM signal of 68.75 µT ± 1.10 µT, which is higher than that registered by the other defects. In addition, Table 3 contains the normal MMM signal variations around the two edges of the five V-shaped notches, considering the maximum and minimum peak values. In the first notch, a shift (27.95 µT ± 1.14 µT) in the normal MMM signal is registered between the two edges of the defect. The second notch has a normal MMM signal shift of 26.4 µT± 0.54 µT. For the third and fourth notches, the normal MMM signal variations were 62.63 µT ± 0.50 µT and 51.98 µT ± 0.64 µT, respectively. On the other hand, the fifth notch achieves a maximum normal MMM signal shift of 71.37 µT ± 0.72 µT. For these normal MMM signals, the first and second notches have the lowest tangential MMM signal variation. The first defect (500 µm depth) generates an alteration of tangential and normal MMM signals around the pipe, which could be used for monitoring its position and size. Figure 13 depicts la maximum variation of tangential MMM signal with respect to the depth of the V-shaped notch. For the first three defects, the maximum variation of this MMM signal increases when the depth increases. For the fourth and fifth defects, the variation of the tangential MMM signal is lower. For instance, the fourth defect has a lower variation with respect to third defect. This could be due to the saturation of the variation of this MMM signal. The fifth defect has a slight increase with respect to the third and fourth defect. Thus, this variation of tangential MMM signal has a nonlinear behavior. Figure 14 depicts the maximum variation of normal MMM signals with respect to the width of the V-shaped notches. In addition, this signal has a nonlinear behavior. The third and fifth width have highest variations of tangential MMM signals. The fourth width has

a variation slightly lower than the third width. For both tangential and normal MMM signals, the third and fifth notches had highest variations. On the other hand, the fourth notch had a small reduction of the variations of the tangential and normal MMM signals in comparison with those of third notch. The five notches had the highest alteration for both MMM signals in comparison with those of the first four notches. Moreover, the maximum variations of tangential MMM signals increased for the first three defects. However, this signal registers a magnetic saturation for the fourth and fifth defect, achieving a small difference in comparison with those of the third defect. Based on the results measured in this work, this MMM method could be used to detect V-shaped notches with depth and width higher that 500 µm. The study about the variations of tangential and normal MMM signals around small V-shaped notches of an ASTM-A36 steel pipe could be used for monitoring the location and size of these defects. The MMM method could be employed for real-time inspection of small V-shaped notches (at scale of a few hundred micrometers) of steel pipes using low-cost equipment and without high-skilled operators.

Table 2. Maximum and minimum values of tangential and normal MMM signals around the center and edges of the five V-shaped notches of an ASTM-A36 steel pipe.

V-Notch Defect	Minimum Tangential (Bz) MMM Signal around Notch Center (µT)	Maximum Normal (By) MMM Signal around Notch Edge (µT)	Minimum Normal (By) MMM Signal around Notch Edge (µT)
S1	-252.8 ± 1.39	71.2 ± 0.66	43.3 ± 0.52
S2	-224.4 ± 1.31	113.8 ± 0.28	87.4 ± 0.40
S3	-202.9 ± 0.90	159.3 ± 0.48	96.7 ± 0.26
S4	-162.4 ± 1.33	87.1 ± 0.86	35.1 ± 0.30
S5	-157.3 ± 0.94	155.2 ± 0.43	83.8 ± 0.41

Table 3. Variations of tangential and normal MMM signals around the center and edges of the five V-shaped notches of an ASTM-A36 steel pipe.

V-Notch Defect	Maximum Variation (ΔBz) of the Tangential MMM Signal around Notch Center (µT)	Maximum Variation (ΔBy) of the Normal MMM Signal between the Edges of Notch (µT)
S1	14.32 ± 1.62	27.95 ± 1.14
S2	16.08 ± 1.86	26.4 ± 0.54
S3	66.73 ± 1.13	62.63 ± 0.50
S4	55.13 ± 1.33	51.98 ± 0.64
S5	68.75 ± 1.10	71.37 ± 0.72

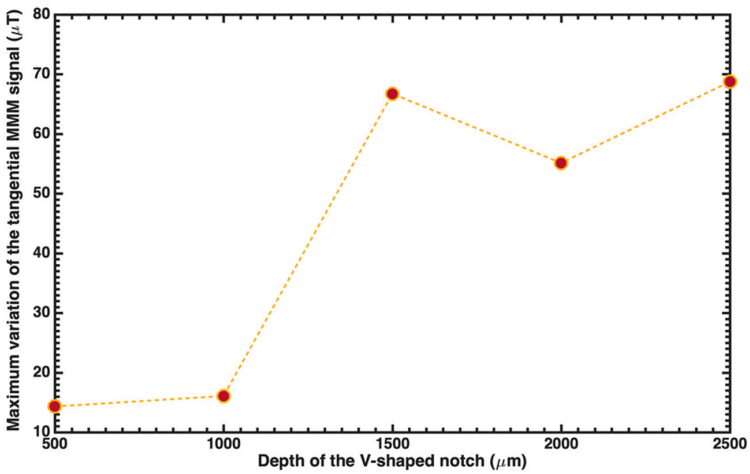

Figure 13. Maximum variation of tangential MMM signals versus depth of the V-shaped notch of the ASTM-A36 steel pipe.

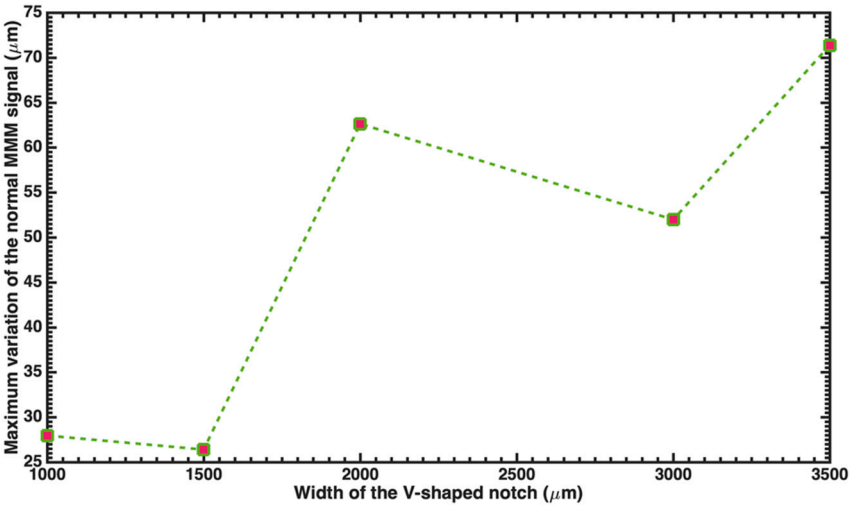

Figure 14. Maximum variation of normal MMM signals versus width of the V-shaped notch of the ASTM-A36 steel pipe.

4. Conclusions

An experimental study of the variations of tangential and normal MMM signals around five small V-shaped notches on the surface of an ASTM-A36 steel pipe was reported. These signals were measured using system formed by a rotational mechanism, a magnetoresistive sensor (MAG3110, Austin, TX, USA, Freescale semiconductor), an Arduino mega (ATmega2560, Santiago, Chile, Arduino) and a data processor. This system does not need expensive equipment, external magnetic field sources and operators with extensive experience. The relationship between the depth and width of each defect with respect to the variations of the tangential and normal MMM signals were studied. The tangential MMM signals around each defect registered a behavior similar to U-shaped curve, which the maximum shift of this signal was related with the defect depth. On the other hand, the normal MMM signals about each defect presented a maximum peak before notch center and a minimum peak after notch center. The separation between these peaks were related to the width of each defect. The smallest defect registered the low shift (14.32 μT ± 1.62 μT and 27.95 μT ± 1.14 μT) of tangential and normal MMM signals in comparison with those of the other notches. The variations of the tangential MMM signals had an increment for the first three defects. However, this signal had a magnetic saturation for the fourth and fifth notch, keeping a small difference in comparison with those of third notch. The largest notch had the highest change (68.75 μT ± 1.10 μT and 71.37 μT ± 0.72 μT) of tangential and normal MMM signals with respect to those of the other defects. The relations between these MMM signals and the size of the V-shaped notches were studied. The MMM method could be used to quantify the size (depth and width) of the V-shaped notch.

In future research, we will consider the influence of the magnetic field due to the stress state of the pipe material.

Author Contributions: Methodology, J.J.V.-S. and J.J.D.-C.; conceptualization, M.A.E.-R. and H.V.-L.; investigation, J.M.-C.; writing—review and editing, A.L.H.-M. All authors have read and agreed to the published version of the manuscript.

Funding: This research received no external funding.

Institutional Review Board Statement: Not applicable.

Informed Consent Statement: Not applicable.

Data Availability Statement: Request should be directed to the corresponding author of this article.

Acknowledgments: This research was supported by project PFCE 2019 "DES Técnica Veracruz" through grant 30MSU0940B-21.

Conflicts of Interest: The authors declare no conflict of interest.

References

1. Mudugamuwa, A.; Jayasundara, C.; Baokun, H.; Amarasinghe, R. Development of a Robotic System with Stand-Alone Monocular Vision System for Eco-friendly Defect Detection in Oil Transportation Pipelines. In *Sustainable Design and Manufacturing*; Smart Innovation, Systems and Technologies; Scholz, S.G., Howlett, R.J., Setchi, R., Eds.; Springer: Singapore, 2021; Volume 200. [CrossRef]
2. Dai, L.S.; Feng, Q.S.; Xiang, X.Q.; Sutherland, J.; Wang, T.; Wang, D.P.; Wang, Z.J. Application of USCCD on girth weld defect detection of oil pipelines. *Appl. Sci.* **2020**, *10*, 2736. [CrossRef]
3. Mevissen, F.; Meo, M. A Review of NDT/Structural Health Monitoring Techniques for Hot Gas Components in Gas Turbines. *Sensors* **2019**, *19*, 711. [CrossRef] [PubMed]
4. Masri, Y.E.; Rakha, T. A scoping review of non-destructive testing (NDT) techniques in building performance diagnostic inspections. *Constr. Build. Mater.* **2020**, *265*, 120542. [CrossRef]
5. Piri, B.; Amini, R.; Asadinia, E.; Vardak, S.; Mehdilouee, R.; Mojarrad, A. Investigation of failure mechanisms and remaining life prediction of firewater pipelines used in industrial applications. *Eng. Fail. Anal.* **2021**, *124*, 105301. [CrossRef]
6. Lorenzo, C.; Janko, S.; Gianluca, R.; Miha, B. Thermoelasticity-based modal damage identification. *Inter. J. Fatigue* **2020**, *137*, 105661. [CrossRef]
7. Yan, W.-J.; Chronopoulos, D.; Papadimitriou, C.; Cantero-Chinchilla, S.; Zhu, G.-S. Bayesian inference for damage identification based on analytical probabilistic model of scattering coefficient estimators and ultrafast wave scattering simulation scheme. *J. Sound Vib.* **2020**, *468*, 115083. [CrossRef]
8. Dehui, W.; Zhitian, L.; Xiaohong, W.; Lingxin, S. Composite magnetic flux leakage detection method for pipelines using alternating magnetic field excitation. *NDT E Inter.* **2017**, *91*, 148–155. [CrossRef]
9. Gholizadeh, S. A review of non-destructive testing methods of composite materials. *Procedia Struct. Integr.* **2016**, *1*, 50–57. [CrossRef]
10. Liu, J.; Xu, G.; Gu, X.; Zhou, G. Ultrasonic test of resistance spot welds based on wavelet package analysis. *Ultrasonics* **2015**, *56*, 557–565. [CrossRef] [PubMed]
11. Purna-Chandra-Rao, B. Non-destructive Testing and Damage Detection. In *Aerospace Materials and Material Technologies*; Prasad, N., Wanhill, R., Eds.; Indian Institute of Metals Series; Springer: Singapore, 2017; Volume 2, pp. 209–218, ISBN 978-981-10-2143-5. [CrossRef]
12. García-Martín, J.; Gómez-Gil, J.; Vázquez-Sánchez, E. Non-destructive techniques based on Eddy current testing. *Sensors* **2011**, *11*, 2525–2565. [CrossRef] [PubMed]
13. Zhang, W.; Shi, Y.; Li, Y.; Luo, Q. A study of quantifying thickness of ferromagnetic pipes based on remote field Eddy current testing. *Sensors* **2018**, *18*, 2769. [CrossRef] [PubMed]
14. Abdalla, A.; Alo, K.; Paw, J.K.S.; Rifai, D.; Faraj, M.A. A novel Eddy current testing error compensation technique based on Mamdani-type fuzzy coupled differential and absolute probes. *Sensors* **2018**, *18*, 2108. [CrossRef] [PubMed]
15. Senck, S.; Scheerer, M.; Revol, V.; Plank, B.; Hannesschläger, C.; Usenbauer, C.; Kastner, J. Microcrack characterization in loaded CFRP laminates using quantitative two- and three-dimensional X-ray dark-field imaging. *Compos. Part A Appl. Sci. Manuf.* **2018**, *115*, 206–214. [CrossRef]
16. Yang, R.; He, Y.; Zhang, H. Progress and trends in nondestructive testing and evaluation for wind turbine composite blade. *Renew. Sust. Energ. Rev.* **2016**, *60*, 1225–1250. [CrossRef]
17. Lu, Q.Y.; Wong, C.H. Applications of non-destructive testing techniques for post-process control of additively manufactured parts. *Virtual Phys. Prototyp.* **2017**, *12*, 301–321. [CrossRef]
18. Antipov, A.G.; Markov, A.A. 3D simulation and experiment on high speed rail MFL inspection. *NDT E Int.* **2018**, *98*, 177–185. [CrossRef]
19. Witek, M. Validation of in-line inspection data quality and impact on steel pipeline diagnostic intervals. *J. Nat. Gas Sci. Eng.* **2018**, *56*, 121–133. [CrossRef]
20. Xu, K.; Qiu, X.; Tian, X. Theoretical investigation of metal magnetic memory testing technique for detection of magnetic flux leakage signals from buried defect. *Nondestruct. Test. Eval.* **2018**, *33*, 45–55. [CrossRef]
21. Dubov, A.; Kolokolnikov, S. Assessment of the material state of oil and gas pipeline based on the metal magnetic memory method. *Welding World* **2012**, *56*, 11–19. [CrossRef]
22. Li, Y.; Zeng, X.; Wei, L.; Wan, Q. Characterizations of damage induced magnetization for X80 pipeline steel by metal magnetic memory testing. *Inter. J. Appl. Electromagn. Mech.* **2017**, *1*, 23–35. [CrossRef]
23. Pengpeng, S.; Ke, J.; Xiaojing, Z. A magnetomechanical model for the magnetic memory method. *Int. J. Mech. Sci.* **2017**, *124–125*, 229–241. [CrossRef]
24. Liu, B.; Fu, P.; Li, R.; He, P.; Dong, S. Influence of crack size on stress evaluation of ferromagnetic low alloy steel with metal Magnetic Memory Technology. *Materials* **2019**, *12*, 4028. [CrossRef] [PubMed]

25. Su, S.; Zhao, X.; Wang, W.; Zhang, X. Metal magnetic memory inspection of Q345 steel specimens with butt weld in tensile and bending test. *J. Nondestruct. Eval.* **2019**, *38*, 64. [CrossRef]
26. Shi, P.; Su, S.; Chen, Z. Overview of researches on the nondestructive testing method of metal magnetic memory: Status and challenges. *J. Nondest. Eval.* **2020**, *39*, 43. [CrossRef]
27. Villegas-Saucillo, J.J. Detección de Defectos Geométricos en Tubos Ferromagnéticos Mediante Procesamiento Digital de Señales con el Método de memoria Magnética. Ph.D. Thesis, Instituto Tecnológico de Celaya, Guanajuato, Mexico, 2019.